Thin Solid Films 520 (2011) 212–216

Contents lists available at ScienceDirect

Thin Solid Films

journal homepage: www.elsevier.com/locate/tsf

Growth behavior and optical properties of N-doped Cu_2O films

H.J. Li, C.Y. Pu, C.Y. Ma, Sh. Li, W.J. Dong, S.Y. Bao, Q.Y. Zhang *

Key Laboratory of Materials Modification by Laser, Ion Electron Beams, Dalian University of Technology, Dalian 116024, People's Republic of China

ARTICLE INFO

Article history:
Received 18 November 2010
Received in revised form 12 July 2011
Accepted 15 July 2011
Available online 23 July 2011

Keywords:
Cuprous oxide
Nitrogen doping
Growth mechanism
Optical properties
Sputtering
Surface morphology

ABSTRACT

N-doped Cu_2O films are deposited by sputtering a CuO target in the mixture of Ar and N_2. The structures zand optical properties have been studied for the films deposited at different temperatures. It is found that N-doping can suppress the formation of CuO phase in the films. The films are highly (100) textured at low temperatures and gradually change to be highly (111) textured at the temperature of 500 °C. With the analysis of (111) and (100) grain sizes, the surface free energy and grain size of critical nuclei are suggested to dominate the film texture. The analysis of the atomic force microscopy shows that the film growth can be attributed to the surface-diffusion-dominated growth. The forbidden rule of band gap transition is found disabled in the N-doped Cu_2O films, which can be attributed to the occupation of 2*p* electrons of nitrogen at the top of valence band. The optical band gap energy is determined to be 2.52 ± 0.03 eV for the films deposited at different temperatures.

© 2011 Elsevier B.V. All rights reserved.

1. Introduction

Cuprous oxide (Cu_2O), a *p*-type direct band-gap semiconductor, is a material of interest in the optoelectronic devices based on oxide semiconductors. Cu_2O has a band gap energy of ~2.1 eV[1–3] and exhibits a Hall mobility exceeding 100 $cm^2\,V^{-1}\,s^{-1}$ [3]. As a *p*-type semiconductor, Cu_2O has also been regarded as one of the most promising materials for application in photovoltaic cells. In the past ten years, Cu_2O has received more attention because of its high absorption coefficient, non-toxicity and low cost producibility [4–10]. Reactive magnetron sputtering is believed to be one of attractive techniques in the fabrication of optoelectronic devices and solar cells. However, it is found that oxygen flux is a key parameter to obtain Cu_2O films by sputtering a metallic Cu target and a precise phase control between Cu_2O and CuO is necessary in the preparation [4]. On the other hand, the sputtered Cu_2O films have the poor optical properties, low Hall mobility (less than 1 $cm^2\,V^{-1}\,s^{-1}$) [4], and low carrier concentration (less than $10^{15}\,cm^{-3}$) [10]. The electric properties of the films should be improved by doping foreign atoms for the applications in optoelectronic devices and photovoltaic cells.

Nitrogen is widely accepted as a nontoxic, low-cost, and easily available material, and can be regarded as an acceptor-type dopant in Cu_2O films if it is substitutionally incorporated into the O lattice sites. In 2001, Ishizuka et al. [5] first reported N-doped Cu_2O films by sputtering a metal copper target in the mixing ambient of Ar, O_2, and N_2 gasses with a reactive radio-frequency (RF) magnetron sputtering method. It was found that the carrier concentration could be controlled from 1×10^{15} to about $10^{17}\,cm^{-3}$ and the Hall mobility was as high as ~50 $cm^2\,V^{-1}\,s^{-1}$. In 2009, Nakano et al. [10] found the optical band-gap energy of N-doped Cu_2O films was enlarged from ~2.1 to ~2.5 eV, which was different from Ishizuka et al.'s results [5]. On the other hand, the role of nitrogen in the film growth has not been investigated by now.

By our knowledge, the Cu_2O films in literature are mainly deposited by sputtering metal copper target in the mixing ambient of Ar and O_2 gasses, in which a precise control of oxygen flux is necessary to obtain Cu_2O films. Nitrogen doping will result in more difficulties in the control of film growth. In this paper, N-doped Cu_2O films are first deposited by sputtering a ceramic CuO target in the mixture of Ar and N_2 at different temperatures. It is found that the nitrogen doping can efficiently suppress the formation of CuO phase. By analyzing the film texture and sizes of (111) and (100) grains, the influences of deposition temperature on the growth behavior of the films are discussed. The band gap energy of N-doped Cu_2O films deposited at different temperatures is determined to be 2.52 ± 0.03 eV.

2. Experimental details

N-doped Cu_2O films were deposited on the quartz substrates by sputtering a CuO target with a reactive rf magnetron sputtering system. The substrates were carefully cleaned by ultrasound in acetone and alcohol for 10 min in order and followed by rinsing in deionized water and dried under flowing N_2 gas. The vacuum chamber was evacuated to 6.3×10^{-4} Pa using a turbomolecular pump. Cu_2O films were deposited at 1 Pa in an ambient atmosphere of Ar and N_2 mixture with the purities of 99.999% at the fluxes of 30 and

* Corresponding author. Tel.: +86 411 84707930; fax: +86 411 84708389.
E-mail address: qyzhang@dlut.edu.cn (Q.Y. Zhang).

0040-6090/$ – see front matter © 2011 Elsevier B.V. All rights reserved.
doi:10.1016/j.tsf.2011.07.037

0 to 6 sccm (standard cubic centimeter per minute), respectively. Deposition was carried out at 60 W for 2 h. The substrate temperature was varied from room temperature (RT) to 500 °C.

X-ray diffraction (XRD) in θ–2θ scan was used to characterize the structure of the films on a diffractometer of Bruker D8 Discover with a Cu K_{α} ($\lambda = 0.15418$ nm) radiation. The atomic force microscopy (AFM) in contact mode was used to analyze the morphological feature on a CSPM5500 scanning probe microscope. The AFM tip is Si_3N_4 tip with force constant of 0.2 N/m. The transmission spectra of Cu_2O films were measured on an Ocean MAYA2000PRO ultraviolet–visible spectrometer at room temperature.

3. Results and discussion

3.1. Structural characterization and growth behavior

Fig. 1 shows the XRD results of Cu_2O films deposited at 500 °C and at different N_2 fluxes. Both of CuO and Cu_2O phases can be observed in the film deposited without nitrogen doping. In the films deposited with nitrogen doping, however, no CuO phase can be found, indicating that N-doping is responsible for the suppression of CuO phase. Cu_3N phase is first observed in the film deposited at the N_2 flux of 4.5 sccm, and the film converts to be a pure Cu_3N phase at 6 sccm, suggesting that the nitrogen content in the ambient atmosphere is a key factor to stabilize the Cu_2O phase.

Fig. 2 shows the XRD results of Cu_2O films deposited at different temperatures and at the N_2 flux of 3 sccm. Two diffraction peaks corresponding to Cu_2O (111) and (100) planes are observed and no diffraction peak related to Cu_3N or CuO is found in the films, indicating that the unique N-doped Cu_2O films can be synthesized at different temperatures. For the films deposited at different temperatures, the intensities of (200) and (111) diffraction peaks are varied with the

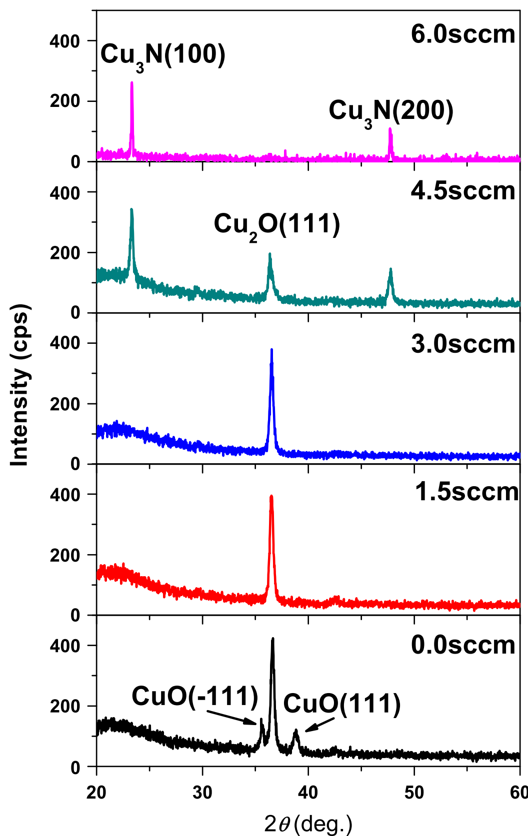

Fig. 1. XRD patterns of Cu_2O films deposited at 500 °C with different N_2 fluxes.

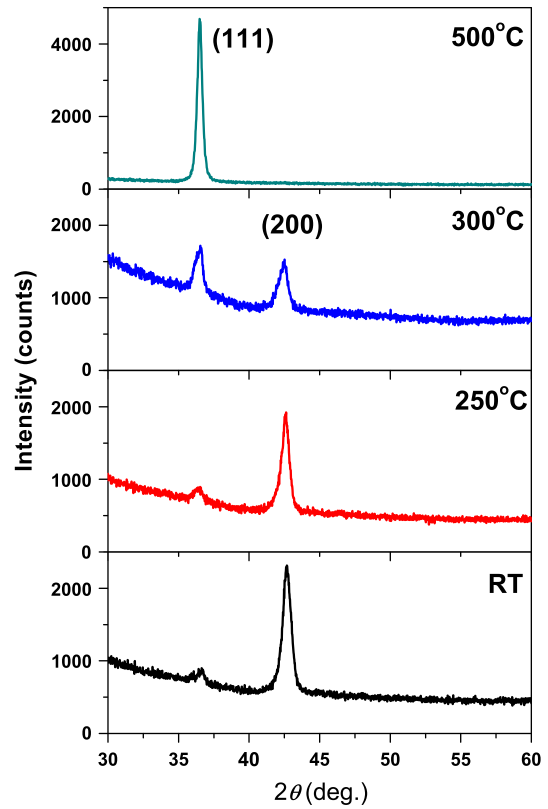

Fig. 2. XRD patterns of N-doped Cu_2O films deposited at different temperatures.

temperature, suggesting that the deposition temperature dominates the texture and the growth behavior of films.

To understand the effects of the deposition temperature in the film growth, the texture factors and grain sizes of the films are calculated. For the films having only two kinds of grains, the texture factor can be defined as [11],

$$f = 1 - 2a/(x + a) \quad (1)$$

where $x = I^{(111)}/I^{(200)}$ and $a = I_0^{(111)}/I_0^{(200)}$, respectively. $I^{(hkl)}$ and $I_0^{(hkl)}$ are the intensities of (hkl) diffraction peak of the as-grown films and Cu_2O powders given in ASTM card (78-2076), respectively. If the film is highly (111) textured, $x \to \infty$ and $f \to +1$, while the film is highly (100) textured, $x \to 0$ and $f \to -1$. The grain sizes can be estimated with Scherrer formula [12]. The texture factor f(111) and grain sizes of the films are plotted as the functions of $1/T$ in Fig. 3, where T is the deposition temperature. We can see that the films are highly (100)

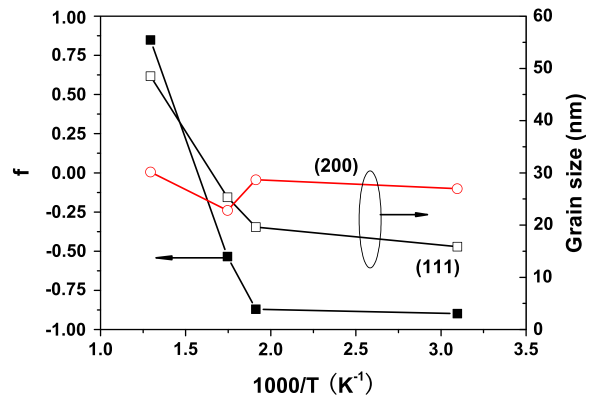

Fig. 3. Temperature dependence of textured factor f and grain sizes.

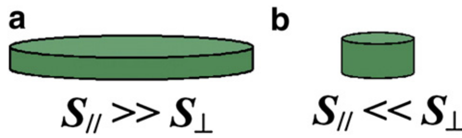

Fig. 4. Schematic of nuclei with different shapes.

textured at the low temperatures. With increasing the deposition temperature up to 500 °C, the films gradually change to be highly (111) textured. The transition takes place at a temperature between 300 and 500 °C. Interestingly, for the films deposited at low temperatures, the (111) grains are smaller than (100) grains. With increasing the deposition temperature up to 500 °C, however, (111) grains gradually change to be larger than (100) grains, indicating that the texture of the films might be dependent on the critical size of different grains in the nucleation stage if the (111) and (100) grains have an approximate growth rate in the nucleation stage.

According to the theory of film growth [13], grains in films will grow up with the lowest surface energy. For the cubic crystals, the order of the surface energy density used to be (111)<(100)<(110). However, the films deposited at different conditions have very different texture instead of only (111) texture, such as the film texture is dependent on the deposition temperature in our case. To understand the growth behavior of the films, a growth model of textured films is suggested on the basis of surface energy density and geometric shapes of grains. In the nucleation stage, the nuclei should have a certain geometric shape instead of a spherical cap. For simplification, the nuclei are supposed to be columnar (as shown in Fig. 4) and the total surface energy of a nucleus is given by

$$E = {}_{\perp}S_{\perp} + {}_{//}S_{//} \tag{2}$$

where $\sigma_{\perp}$ and $\sigma_{//}$ are the surface energy densities of the surfaces vertical and parallel to the substrate surface, respectively. $S_{\perp}$ and $S_{//}$ are the areas of the corresponding surfaces. We can see that the total surface energy of a nucleus is dependent on both of surface area and surface energy density. For the larger nuclei, as shown in Fig. 4(a) and corresponding to the deposition at high temperatures in our case, $S_{//}$ is much larger than $S_{\perp}$ because the heights of nuclei are only several atomic layers and the nucleus with smallest $\sigma_{//}$ will have the lowest E. In our case, Cu_2O is cubic crystal and (111) planes have the lowest surface energy density. Therefore, the films deposited at high temperature are preferred growth with (111) texture. In the case of low temperature, the critical sizes of nuclei are not large enough. If $S_{//}>S_{\perp}$, the nuclei with the smallest $\sigma_{//}$ are preferred. However, if $S_{//}<S_{\perp}$, as shown in Fig. 4(b), the nuclei with the larger $\sigma_{//}$ are preferred. The mechanism is consistent with our experiment results and is helpful to understand the film growth in other cases. For example, in the ion beam assistant deposition and in the plasma enhanced deposition with negative bias voltage, the films textured with high surface energy density are much easier obtained than the films deposited without ion bombardment [14]. One of the important reasons can be attributed to the reduction of critical sizes of the nuclei due to the ion bombardment.

3.2. Surface morphology and scaling analysis

Fig. 5 shows the AFM images of Cu_2O films in a scale of $2\times2\ \mu m^2$. With the increase of deposition temperatures, the grain size and the roughness of the films gradually increased and the grain density gradually decreased. The surface morphology has an irregular geometry with self-affine structure determined by the thermodynamic environment. The surface morphology exhibits both spatial and temporal scaling behaviors over a large variation of dynamic length scale. The scaling behavior can be investigated by using the one-dimensional power spectral density (1DPSD) of an AFM topological profile defined as [15–17],

$$\mathrm{1DPSD}(f) = \frac{1}{L}\left|\int_0^L y(x)e^{i2\pi fx}dx\right|^2. \tag{3}$$

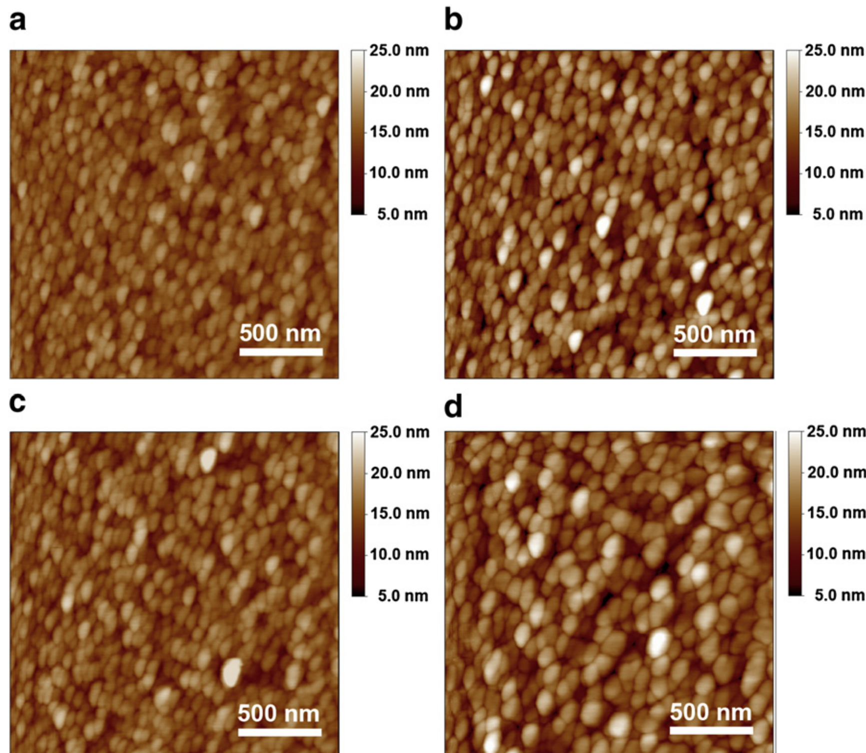

Fig. 5. AFM surface morphologies of N-doped Cu_2O films at (a) room temperature, (b) 250 °C, (c) 300 °C, (d) 500 °C.

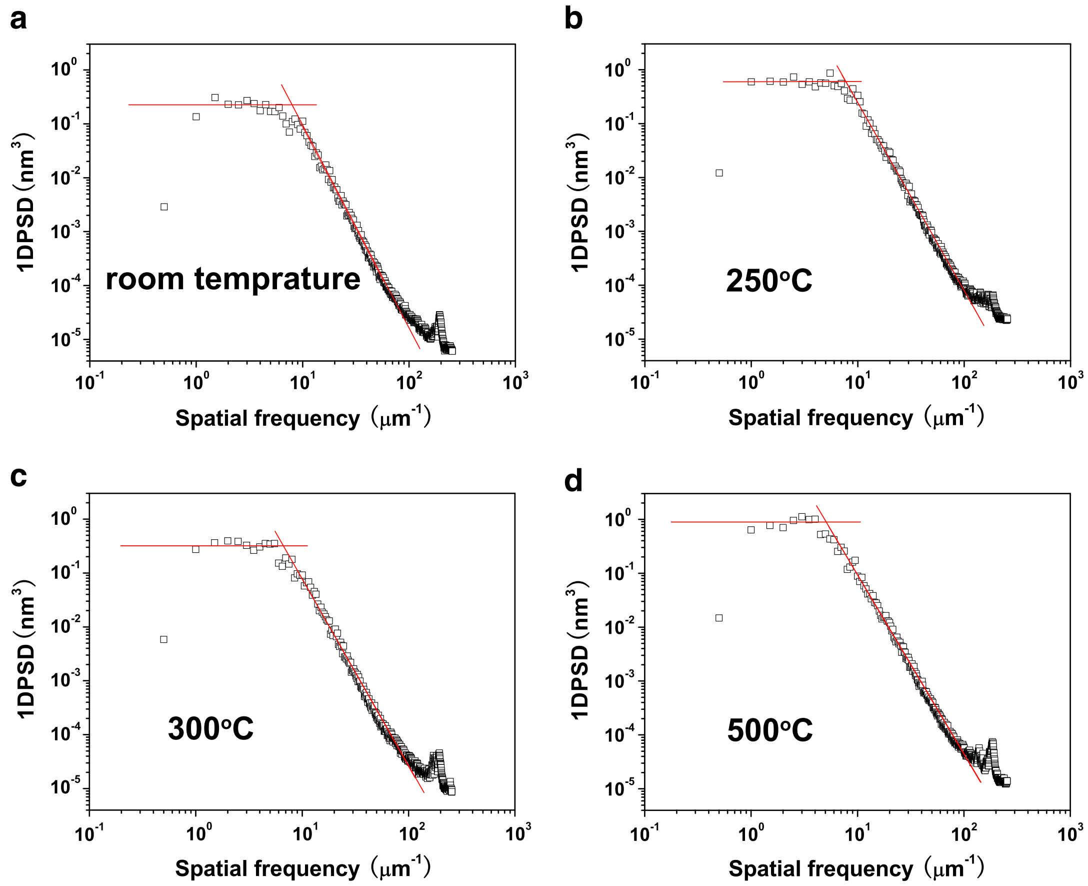

Fig. 6. 1DPSD spectra of N-doped Cu_2O films at (a) room temperature, (b) 250 °C, (c) 300 °C, (d) 500 °C.

where $y(x)$ is the topographical profile, L is the scan length, f is the spatial frequency, and x is the fast scan direction of the image. The log–log 1DPSD plots of the AFM topographical morphologies corresponding to Fig. 5 are presented in Fig. 6. The 1DPSDs exhibit a frequency-dependent region with power-low decay $1DPSD(f) \propto f^{-\gamma}$ [17,18]being indicative of a self-affine structure, and a plateau 1DPSD $(1/L)$ at low spatial frequencies corresponding to the absence of non-local correlation along the line scan. For the frequency-dependent region, the roughness scaling exponent α is related to γ by $\alpha = (\gamma - d)/2$ [17,18], where d is the line scan dimension. The correlation length of a self-affine structure, which is the range corresponding to the intersection between the self-affine branch and the plateau, is determined by [15]

$$\xi = \exp\left\{\frac{ln[1DPSD(1/L)] - lnK_0}{\gamma}\right\} \tag{4}$$

where K_0 is a constant. The low-frequency plateau $1DPSD(1/L)$ is related to the saturation roughness, which represents the lack of the local association on the low frequency.

By fitting frequency-dependent region in a line, the spatial scaling exponent γ is determined to be 3.76, 3.48, 3.46, and 3.32 for the films deposited at RT, 250, 300, and 500, respectively, and the corresponding roughness exponent α is 1.38, 1.24, 1.23, and 1.16. $\alpha > 1$ means that the roughening fluctuations and the smoothing effects cannot reach a balance, and the local surface slope increases with time. The high-frequency region is characterized by anomalous dynamic scaling behavior dominated by surface diffusion [18]. The correlation length is determined to be 123, 129, 155, and 197 nm for the films deposited temperature at RT, 250, 300, and 500 °C, respectively, which has a close relationship with the grain sizes and texture factor of the films.

3.3. Optical properties and optical band-gap energy

Fig. 7(a) shows the transmission spectra of the films deposited at different temperatures. The films exhibit a high transmittance from visible to the infrared wavelength range (500–1100 nm). By fitting the transmittance with Sellmeier's optical model, the thickness is determined to be 337, 285, 250, and 331 nm for the films deposited at RT, 250, 300, and 500 °C, respectively. With the transmittance and the determined thickness of the films, the absorption coefficient (α) can be calculated and the optical band gap energy (E_g) can be determined, as shown in Fig. 7(b).

Cu_2O is a direct band-gap semiconductor, but the direct transition from the top of valence band to the bottom of conduction band is forbidden. According to the theory of energy band, the value of E_g should be determined with the relationship of [19]

$$\alpha \propto \left(h\nu - E_g\right)^{3/2} / h\nu, \tag{5}$$

where $h\nu$ is the incident photon energy. However, Nakano et al. found that the absorption coefficient of N-doped Cu_2O films was close to the relationship of [19]

$$\alpha \propto \left(h\nu - E_g\right)^{1/2}. \tag{6}$$

Similarly, our results can also be fitted with Eq. (6) well instead of Eq. (5), suggesting that the forbidden rule of the transition for Cu_2O is disabled in the films of N-doped Cu_2O. Our first-principle calculations (not shown here) show that the 2p electrons of N atom occupy the top region of valence band, which should be the reason for changing the

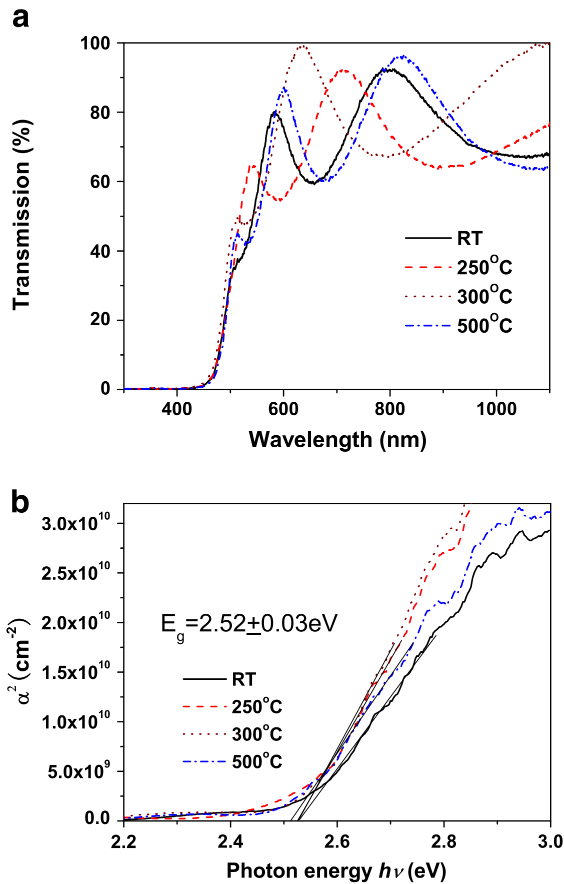

Fig. 7. (a) Transmittance spectra of N-doped Cu_2O films at different temperatures. (b) Relationship of $\alpha^2 \propto h\nu - E_g$ for the films deposited at different temperatures.

transition rule of N-doped Cu_2O because the wave function of p electron is odd.

With the relationship given in Eq. (6), the E_g value is determined to be 2.52 ± 0.03 eV for the films deposited at different temperatures, which is consistent with most of N-doped Cu_2O films reported in the literature [10,20,21], but different from Ishizuka et al.'s results, where no significant band-edge shift was found for the films deposited in the different N_2 fluxes [5]. Our first-principle calculations demonstrate that N-doping enlarges the band gap energy about 25%, being very close to the experimental results of 20%. Nakano et al. found that the N-doping concentration was in the range of 2% to 3% for the films deposited with different N fluxes and the optical band gap energy was enlarged from about 2.1 to 2.5 eV [10]. Our results suggest that the deposition temperature cannot affect the band gap energy significantly at the given N_2 fluxes, which might be attributed to the limitation of N content in the films according to the results reported by Nakano et al. [10].

4. Conclusions

N-doped Cu_2O films deposited in the mixture of Ar and N_2 by sputtering a CuO target are highly (100) textured at the low deposition temperatures, and gradually change to be highly (111) textured at the deposition temperature of 500 °C. A growth model of the films is given to explain the change of film texture with deposition temperature. AFM analysis shows that all the films deposited at different temperatures have the spatial scaling exponents greater than 1 and the film growth can be attributed to the surface-diffusion-dominated growth. The spatial scaling exponent and characteristic length of the film surface morphologies are found to correlate to the grain sizes and textured factors of the films. The forbidden rule of band gap transition is disabled in the N-doped Cu_2O films, which can be attributed to the occupation of 2p electrons of nitrogen at the top of valence band. The optical band gap energy is determined to be 2.52 ± 0.03 eV for the films deposited at different temperatures.

Acknowledgments

The work is supported by the National Natural Science Foundation of China under grant no. 10774018 and the Key Basic Research Project from the Ministry of Science and Technology of China under grant no. 2007CB616902.

References

[1] A. Roos, T. Chibuye, B. Karlsson, Solid Energy Mater. 7 (1983) 453.
[2] J. Ghisjen, L.H. Tjeng, J. Elp, H. Eskes, Phys. Rev. B 38 (1988) 11322.
[3] K. Matsuzaki, K. Nomura, H. Yanagi, T. Kamiya, M. Hirano, Appl. Phys. Lett. 93 (2008) 202107.
[4] S. Ishizuka, T. Maruyama, K. Akimoto, Jpn. J. Appl. Phys. 39 (2000) L786.
[5] S. Ishizuka, S. Kato, T. Maruyama, K. Akimoto, Jpn. J. Appl. Phys. 40 (2001) 2765.
[6] S. Ishizuka, S. Kato, Y. Okamoto, K. Akimoto, J. Cryst. Growth 237–239 (2002) 616.
[7] N. Kikuchi, K. Tonooka, Thin Solid Films 486 (2005) 33.
[8] Y.M. Lu, C.Y. Chen, M.H. Lin, Mater. Sci. Eng. B 118 (2005) 179.
[9] K. Akimoto, S. Ishizuka, M. Yanagita, Y. Nawa, K.P. Goutam, T. Sakurai, Solid Energy 80 (2006) 715.
[10] Y. Nakano, S. Saeki, T. Morikawa, Appl. Phys. Lett. 94 (2009) 022111.
[11] H. Rudigier, E. Bergmann, J. Vogel, Surf. Coat. Technol. 36 (1988) 75.
[12] S. Fujihara, C. Sasaki, T. Kimura, J. Eur. Ceram. Soc. 21 (2001) 2109.
[13] M. Ohring, Materials Science of Thin Films: Deposition and Structure, Academic Press, 2002.
[14] W.J. Fu, Z.W. Liu, J.F. Gu, M. Liu, Q.Y. Zhang, J. Inorg. Mater. 24 (2009) 602 (in Chinese).
[15] F. Biscarini, P. Samori, O. Greco, R. Zamboni, Phys. Rev. Lett. 78 (1997) 2389.
[16] A.E. Lita, J.E. Sanchez, J. Appl. Phys. 85 (1999) 876.
[17] H.H. Zhang, C.Y. Ma, Q.Y. Zhang, Vacuum 83 (2009) 1311.
[18] A.E. Lita, J.E. Sanchez, Phys. Rev. B 61 (2000) 7692.
[19] X.C. Shen, Spectra and Optical Properties of Semiconductors, Chinese Academic Press, 2002 (in Chinese).
[20] S. Han, H.Y. Chen, L.T. Kuo, C.H. Tsai, Thin Solid Films 517 (2008) 1195.
[21] Y.H. Zhang, Master Thesis of Zhejiang University, Preparation of p-type Cu2O thin films by DC magnetron sputtering, 2007 (in Chinese).